ISSN 1063-7737, Astronomy Letters, 2023, Vol. 49, No. 8, pp. 475–485. © Pleiades Publishing, Inc., 2023.
Russian Text © The Author(s), 2023, published in Pis'ma v Astronomicheskii Zhurnal, 2023, Vol. 49, No. 8, pp. 562–572.

SDSS J085414.02+390537.3—a New Asynchronous Polar

A. I. Kolbin[1,2,3*], M. V. Suslikov[1,2], V. Yu. Kochkina[1,2], N. V. Borisov[1], A. N. Burenkov[1], and D. V. Oparin[1]

[1] *Special Astrophysical Observatory, Russian Academy of Sciences, Nizhnii Arkhyz, Karachai-Cherkessian Republic, 357147 Russia*

[2] *Kazan (Volga Region) Federal University, Kazan, 420000 Russia*

[3] *North-Caucasus Federal University, Stavropol, 355017 Russia*

Received July 24, 2023; revised August 24, 2023; accepted August 24, 2023

Abstract—Based on data from the ZTF photometric survey, we have revealed asynchrony of the polar SDSS J085414.02+390537.3. A beat period $P_{\rm beat} = 24.6 \pm 0.1$ days, during which the system changes its brightness by $\approx 3^m$, is distinguished in the light curves. Power peaks at the white-dwarf rotation period $P_{\rm spin} = 113.197 \pm 0.001$ min and orbital period $P_{orb} = 113.560 \pm 0.001$ min are revealed in the periodograms, with the corresponding polar asynchrony being $1 - P_{\rm orb}/P_{\rm spin} = 0.3\%$. The photometric behavior of the polar points to a change of the main accreting pole during the beat period. Based on the Zeeman splitting of the Hβ line, we have estimated the mean magnetic field strength of the white dwarf to be $B = 28.5 \pm 1.5$ MG. The magnetic field strength near the magnetic pole has been found by modeling the cyclotron spectra to be $B = 34 \pm 2$ MG. The Doppler tomograms in the Hβ line exhibit a distribution of emission sources typical for polars in velocity space with evidence of the transition of the accretion stream from the ballistic trajectory to the magnetic one.

DOI: 10.1134/S1063773723080029

Keywords: *stars: novae, cataclysmic variables; individual: SDSS J085414.02+390537.3; methods: photometry, spectroscopy.*

1. INTRODUCTION

Cataclysmic variables are close binary systems with orbital periods $P_{\rm orb} = 1.4$–9 h that consist of a white dwarf and a low-mass cool star (usually an M dwarf) filling its Roche lobe (Warner 1995; Hellier 2001). The material of the cool component outflows from the inner Lagrange point L_1 and forms an accretion disk in the case of a weak white-dwarf magnetic field ($B \lesssim 0.1$ MG). A different picture of accretion is observed in systems with a strong magnetic field ($B \gtrsim 10$ MG), where ionized gas flows onto the surface of the accretor along magnetic field lines without the formation of an accretion disk. When the infalling gas interacts with the accretor surface, hot ($T \sim 10$ keV) and compact accretion spots are formed, which are the sources of hard X-ray radiation and polarized cyclotron radiation in the optical and near-infrared ranges. Objects of this kind are called AM Her stars or polars (Cropper 1990). In polars the interaction of the strong magnetic field of the accretor with the donor leads to synchronization of the rotation of the white dwarf with its orbital motion ($P_{\rm spin} = P_{\rm orb}$, where $P_{\rm spin}$ is the white-dwarf rotation period). At magnetic fields $B \sim 0.1$–10 MG an accretion disk is formed, which is destroyed from the inside by the white-dwarf magnetic field. These systems are called DQ Her stars or intermediate polars (Patterson 1994). In contrast to polars, DQ Her systems are not synchronous; their rotation-to-orbital period ratios are distributed in a wide range with a mean $P_{\rm spin}/P_{\rm orb} \approx 0.1$[1].

A small group of objects called asynchronous polars is distinguished among the polars. In these systems there is weak asynchrony of the white-dwarf rotation that does not exceed a few percent. By now, asynchrony has been confirmed for V1500 Cyg (Pavlenko et al.2018), V1432 Aql (Littlefield et al. 2015), BY Cam (Silber et al. 1992), CD Ind (Littlefield et al. 2019), SDSS J084617.11+245344.1 (Littlefield et al. 2023), 1RXS J083842.1-282723

*E-mail: kolbinalexander@mail.ru

[1] The catalog of intermediate polars with orbital and rotation periods is accessible on K. Mukai's page: https://asd.gsfc.nasa.gov/Koji.Mukai/iphome/catalog-/members.html

(Halpern et al. 2017), IGR J19552+0044 (Tovmassian et al. 2017), and SDSS J134441.83+204408.3 (Littlefield et al. 2023). It is assumed that this state is unstable and asynchronous systems move toward the state of synchronous motion. It is possible that such systems were brought out of the state of synchronous motion by a recent nova explosion (Stockman et al. 1988). According to present views, a distinguishing feature of asynchronous polars is their temporary stay in the state of asynchrony, whereas for intermediate polars the state with $P_{\rm spin} < P_{\rm orb}$ should be stable (King and Lasota 1991). The difference between the orbital and rotation periods of the white dwarf leads to a periodic change in the geometry of the accretion flows, a drift of the accretion spots over the accretor surface, and a change of the main accreting magnetic pole (Sobolev et al. 2021). The change of the accreting pole and the drift of the spots manifest themselves as variability of the light-curve shape modulated with the white-dwarf rotation during the beat period $P_{\rm beat} = (\omega - \Omega)^{-1}$, where $\omega = 1/P_{\rm spin}$ is the white-dwarf rotation frequency and $\Omega = 1/P_{\rm orb}$ is the orbital frequency (Littlefield et al. 2019, 2023.

The object SDSS J085414.02+390537.3 (hereafter J0854) was assigned by Christian et al. (2001) to the candidates for magnetic cataclysmic variables. Szkody et al. (2005) detected cyclotron harmonics in the spectrum of J0854 whose positions corresponded to a magnetic field strength of 44 MG. A high circular polarization of the radiation reaching 30% was also detected. Dillon et al. (2008) determined the photometric period of the polar, $P = 113.26 \pm 0.03$ min. The light curve had a double-peaked bright phase that was interpreted as the passage of the accretion spot across the white-dwarf disk. We became interested in J0854 after the detection of evidence for asynchrony in the long-term light curves of the ZTF survey. For a more detailed study of this system we analyzed its phase resolved spectroscopy.

This paper is structured as follows. In the second section we describe our spectroscopic observations of J0854 and their reduction. Next, in the third section, we analyze the long-term ZTF light curves of J0854. We investigate the variability at the beat period and the variability modulated by the white-dwarf rotation. In the fourth section we perform an analysis of the spectra for J0854, including the determination of the magnetic field from the Zeeman splitting of the Hβ line, the modeling of the cyclotron spectrum, and Doppler tomography. The results of our work are summarized in the section "Conclusions."

2. OBSERVATIONS AND DATA REDUCTION

A sets of spectra for J0854 was taken with the 6-m BTA telescope at the Special Astrophysical Observatory of the Russian Academy of Sciences on the night from March 7 to 8, 2022, and from April 24 to 25, 2022. On the first and second nights the observations were carried out using the SCORPIO-2 and SCORPIO-1 (Afanasiev and Moiseev 2011) focal reducers, respectively. The mode of long-slit spectroscopy with exposure times of 300 s was used in both cases. On the first observing night we managed to cover only ≈ 0.6 of the polar's orbital period, while on the second night we observed the full period of $\approx$ 110 min. In the March observations we used a volume phase holographic grating, VPHG1200@540, which at a slit width of $1.0''$ gave a spectral resolution $\Delta\lambda \approx$ 5.2 Å and covered the spectral range 3700–7300 Å. The observations were performed under light cloudiness with a $2.5''$ seeing. In the April observations with SCORPIO-1 we used the VPHG1200G grism and a $1.2''$-wide slit, which provided a resolution $\Delta\lambda \approx 5$ Å with the coverage of the wavelength range 3800–5700 Å. These observations were carried out in good astroclimatic conditions with a $1.8''$ seeing.

The observational data were reduced using the IRAF[2] software package. The spectral frames were bias subtracted; a correction for the CCD sensitivity microvariations was made based on flat-field lamp frames. The cosmic-ray hits were removed using the LaCosmic algorithm (van Dokkum 2001). We corrected the geometric distortions and calibrated the spectra in wavelengths using He-Ne-Ar lamp frames. An optimal extraction of the spectra (Horne 1986) with sky background subtraction was carried out. We performed the spectrophotometric calibration based on our observations of the standards Feige 34 (for the March 7/8, 2022 observations) and AGK+81°266 (for the April 24/25, 2022 observations). The fluxes were corrected for variable atmospheric opacity using the spectra of the neighboring star captured by the spectrograph slit. For each spectrum we found the barycentric Julian dates and the barycentric corrections for the radial velocity.

3. ANALYSIS OF ZTF PHOTOMETRY

Variability at the Beat Frequency

The long-term ZTF light curves of J0854 (Masci et al. 2018) spanning almost 4.8 years in the g, r, and i bands are shown in Fig. 1. Fairly rapid (of the order of a month) changes in the brightness of the object from 20^m to 16^m in these three bands can be seen. The same figure shows the Lomb–Scargle periodograms (VanderPlas 2018) constructed from the presented light curves. The power peak at the

[2]The IRAF astronomical data processing and analysis package is accessible at https://iraf-community.github.io.

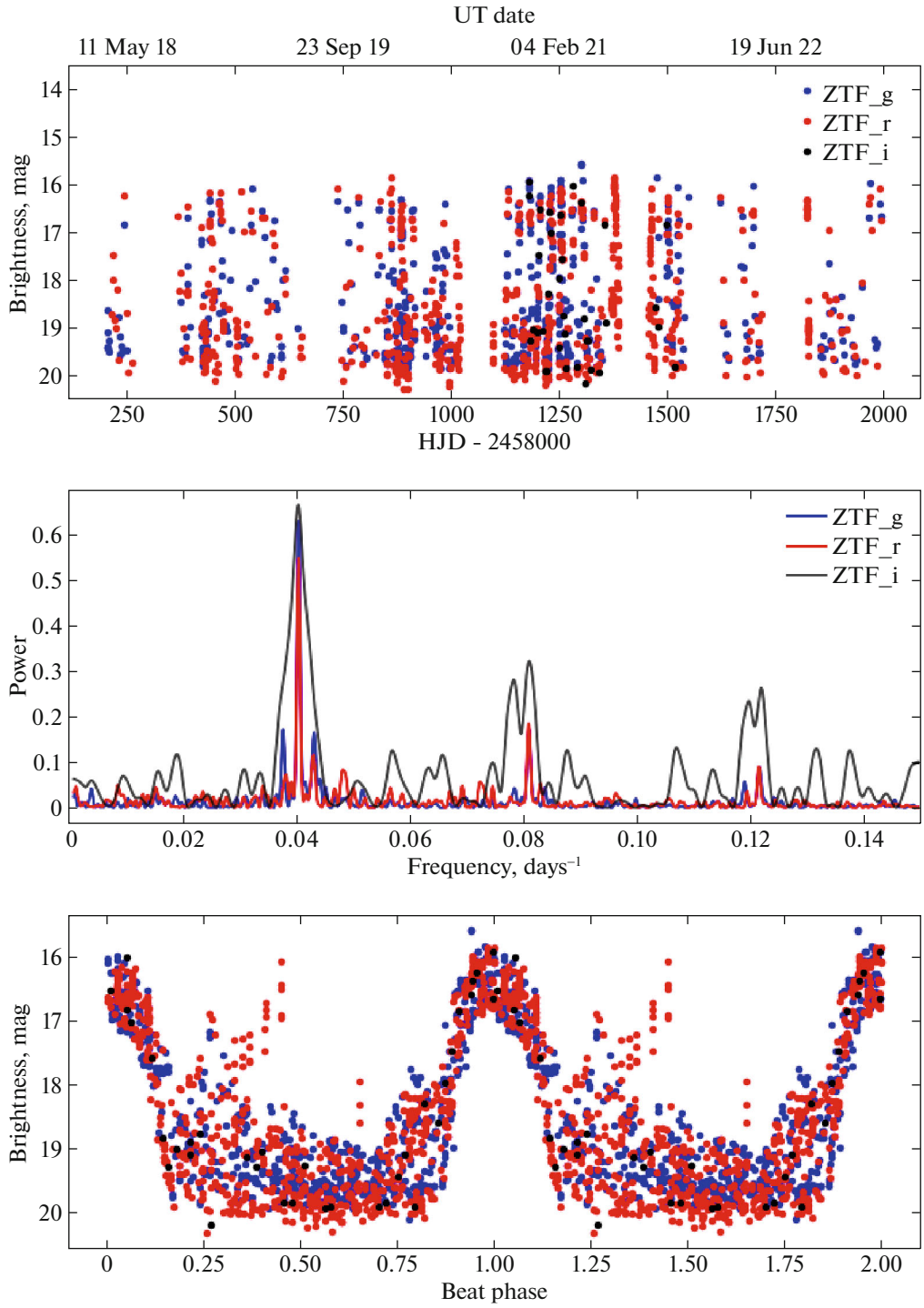

Fig. 1. Upper panel: the long-term ZTF light curves of J0854 in the g, r, and i bands. Middle panel: the Lomb–Scargle periodograms obtained for the light curves in these three bands. Lower panel: the phased light curves constructed from the ephemeris (1).

frequency $f = 0.04060 \pm 0.00023$ day^{-1} (period $P = 24.63 \pm 0.14$ day) revealed by the observational data in the three bands engages our attention. Figure 1 also presents the phased light curves constructed for the period found. They exhibit a high state with a mean brightness $\langle g \rangle \approx \langle r \rangle \approx \langle i \rangle \approx 16.5^m$ and a low state with $\langle g \rangle \approx \langle r \rangle \approx \langle i \rangle \approx 19.5^m$. The regularity of the change in the brightness state is beyond doubt,

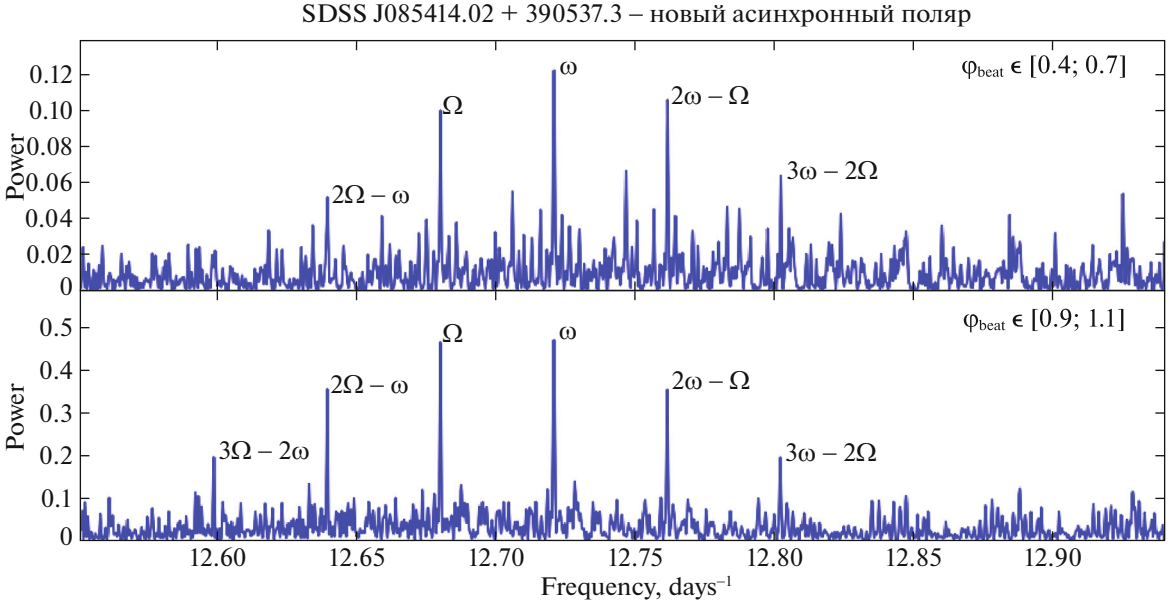

Fig. 2. The periodograms of J0854 near the white-dwarf rotation frequency for the low ($\varphi_{\rm beat} = 0.4{-}0.7$, the upper panel) and high ($\varphi_{\rm beat} = 0.9{-}1.1$, the lower panel) states. The positions of the peaks of the white-dwarf rotation frequency ω, the orbital frequency Ω, and the sidebands are indicated.

but it is atypical for AM Her systems. Obviously, the derived period exceeds considerably the orbital periods of polars ($\sim 1/10$ days), while the observed brightness variability of $\approx 3^m$ is much greater than the amplitude of the out-of-eclipse orbital variability of polars ($\sim 1^m$). An amplitude $\sim 3^m$ is typical for the change in the states of polars due to the variability of the accretion rate. However, this switching of brightness states is irregular and does not exhibit any significant periodicity. We assumed that J0854 is an asynchronous polar and the period found is the beat period $P_{\rm beat} = (\omega - \Omega)^{-1}$. In other words, this period is equal to the rotation period of the white dwarf in the coordinate system rotating with the binary star. The observed brightness variability in this case can be caused by a change of the main accreting magnetic pole (for more details, see the section "Conclusions"). Note that the phased light curve was constructed according to the ephemeris

$$HJD_{\rm beat} = 2459082.49(7) + 24.6(1)E, \qquad (1)$$

where the initial epoch corresponds to the middle of the high state.

Orbital and Rotational Variabilities

To analyze the rapid variability, we selected two beat phase ranges, $\varphi_{\rm beat} = 0.4{-}0.7$ and $\varphi_{\rm beat} = 0.9{-}1.1$, which correspond to the low and high states, respectively (see Fig. 1). These ranges have small brightness dispersions, which gives hope to distinguish the rotational or orbital variability undistorted by the change of the accretion rate in them. Our analysis was carried out in the g and r bands with a preliminary subtraction of the mean brightness. In the range $\varphi_{\rm beat} = 0.4{-}0.7$ the mean brightness was assumed to be constant, while in the range $\varphi_{\rm beat} = 0.9{-}1.1$ it depends strongly on $\varphi_{\rm beat}$ and was found by fitting the light-curve segment with a parabola. The Lomb–Scargle periodograms for the two ranges are presented in Fig. 2. They contain a lot of peaks, the strongest of which corresponds to the period $P_{\rm spin} = 113.197 \pm 0.001$ min close to the white-dwarf rotation period (Dillon et al. 2008). The frequency of the neighboring peak is $\omega - 1/P_{\rm beat}$ and is the orbital frequency Ω, while the corresponding orbital period is $P_{\rm orb} = 0.078861 \pm 0.000001$ day (113.55984 ± 0.001 min). Other power peaks are the sidebands produced by combining the frequencies ω and Ω.

The light curves in the low ($\varphi_{\rm beat} = 0.4{-}0.7$) and high ($\varphi_{\rm beat} = 0.9{-}1.1$) states folded with the white-dwarf rotation period found are shown in Fig. 3. In both bands they have a double-peaked bright phase that apparently results from the change in accretion spot visibility conditions as the white dwarf rotates. The characteristic double-peaked structure of the bright phase in polars is interpreted as anisotropy in the the cyclotron radiation from the accretion spot. It is most intense when the spot is near the edge of

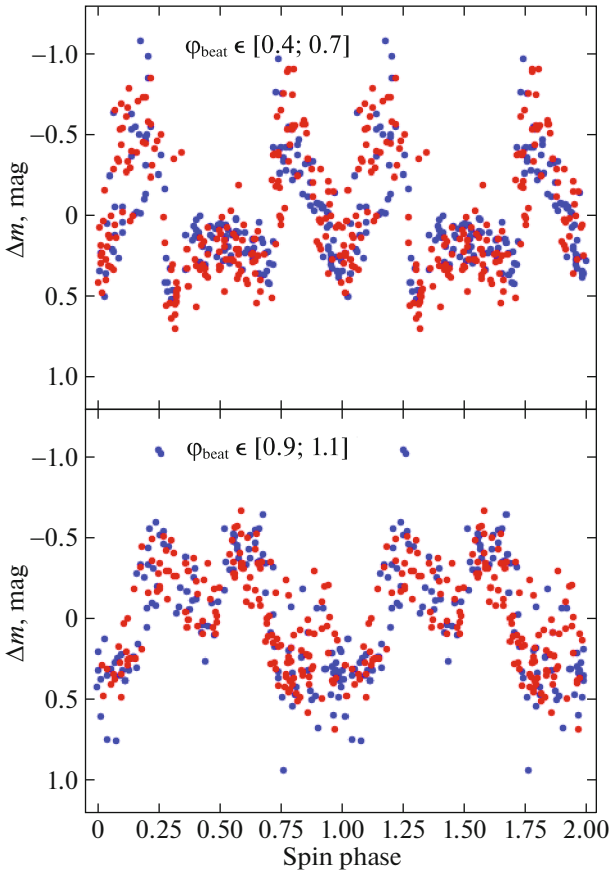

Fig. 3. The phased light curves of J0854 derived from the ephemeris (2) and showing the variability modulated with the white-dwarf rotation. The upper and lower panels show the light curves derived from the low-state, $\varphi_{\rm beat} = 0.4{-}0.7$, and high-state, $\varphi_{\rm beat} = 0.9{-}1.1$, data, respectively. The g- and r-band measurements are indicated by the blue and red dots, respectively.

the white-dwarf disk, i.e., when the angle between the magnetic field lines and the line of sight is close to 90°, and decreases as the spot approaches the disk center (if the stellar rotation axis has a high inclination; for more details, see, e.g., Kolbin and Borisov 2020; Kolbin et al. 2022). To construct the presented phased light curves, we used the ephemeris

$$HJD_{\rm rot} = 2459063.376(3) + 0.0786091(7)E, \quad (2)$$

where the initial epoch corresponds to the middle of the bright phase for $\varphi_{\rm beat} = 0.4{-}0.7$.

The change in the position of the bright phase by $\approx 1/2P_{\rm spin}$ during the transition from the low state to the high one engages our attention. This phenomenon fits well into the picture of J0854 asynchrony and is apparently caused by the change of the main accreting magnetic pole.

4. ANALYSIS OF SPECTRA

Zeeman Splitting

There are Zeeman absorption components of the Hβ line in the spectra of J0854 taken on April 24/25, 2022. The Zeeman splitting is typical for polars at a low accretion rate, when the white-dwarf emission manifests itself in the spectra. A low accretion rate at the time of J0854 observations is suggested by the absence of an intense HeII λ4686 line. Fig. 4 shows the averaged spectrum of J0854 in which the reliably identified Zeeman components are highlighted. The positions of these components were found by Gaussian fitting, and 1σ was taken to be the position error. To estimate the magnetic field of the white dwarf, we calculated the energy spectrum of a hydrogen atom in a strong magnetic field using the code from Schimeczek and Wunner (2014). The Zeeman splitting diagram for the Hα, Hβ, and Hγ lines is also presented in Fig. 4. The average magnetic field of the white dwarf was estimated to be $B = 28.5 \pm 1.5$ MG.

Cyclotron Spectrum

One spectrum with weak cyclotron harmonics stands out in the spectral series obtained on March 7/8, 2022 (see Fig. 5). We modeled it with a

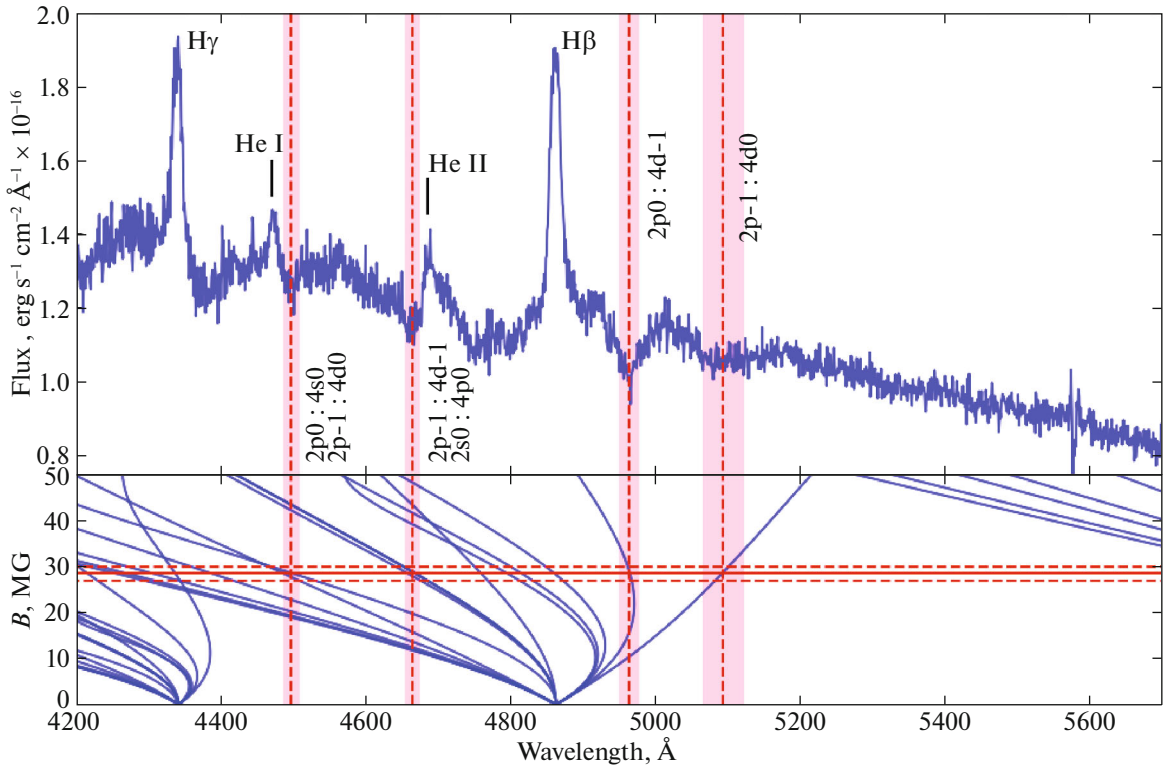

Fig. 4. Upper panel: the averaged spectrum of J0854 obtained from the April 24/25, 2022 observations. The vertical lines indicate the positions of the Zeeman absorption components of the Hβ line; the pink bars indicate the uncertainty in their positions. The identified transitions in the hydrogen atom are also indicated. Lower panel: the Zeeman splitting diagram for the Hα, Hβ, and Hγ lines. The horizontal solid line indicates our estimate of the magnetic field strength.

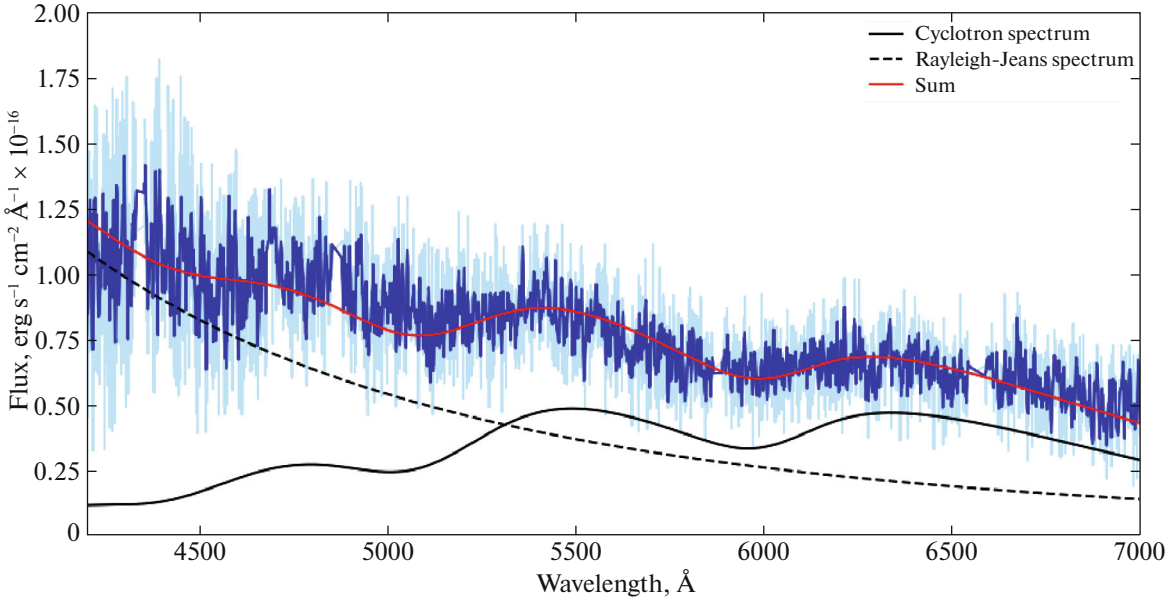

Fig. 5. The spectrum of J0854 with cyclotron harmonics (blue curve, the emission lines were removed) and its fit (red curve) by the sum of the cyclotron spectrum (black curve) and the Rayleigh–Jeans spectrum (black dashed curve). The blue curve indicates the observed spectrum smoothed by the Savitzky–Golay filter.

simple accretion spot model uniform in temperature and density, which is often used to study polars (Campbell et al. 2008; Kolbin et al. 2019; Beuermann et al. 2020). The Rayleigh–Jeans spectrum was added to the cyclotron spectrum to take into account the white-dwarf emission and the possible contribution from the accretion stream. The model depends on four parameters: the magnetic field strength in the spot B, the electron temperature T_e, the angle between the magnetic field lines and the line of sight θ, and the plasma parameter $\Lambda = \omega_p^2 \ell / \omega_c c$, where ω_p is the plasma frequency, ℓ is the depth of the emitting region along the line of sight, and $\omega_c = eB/m_e c$ is the cyclotron frequency. The intensity of the cyclotron radiation was computed using the absorption coefficients calculated by the method of Chanmugam and Dulk (1981). The best fit of the observed spectrum was obtained for a magnetic field strength $B \approx 34$ MG. Note that the noisiness of the spectra gives an uncertainty in the positions of the cyclotron components ≈20 Å, which corresponds to an error in the magnetic field strength ~ 0.1 MG. The degeneracy of the solution in temperature and plasma parameter (Campbell et al. 2008) makes a much larger contribution to this error. Unfortunately, the temperature T_e and the plasma parameter Λ cannot be determined simultaneously by modeling the cyclotron spectrum due to their similar influence on the shape of the spectrum. We varied the temperature in the range 5–20 keV that encompasses the values of this parameter typical for polars. For all temperatures in this range we found the solution that described best the observed spectrum by the least-squares method. In this case, the magnetic field strength changed by ≈2, which was taken as the error in the magnetic field. The optimal values of the plasma parameter lay in the range from $\log \Lambda = 4$ (for T_e keV) to $\log \Lambda = 7$ (for $T_e = 5$ keV) expected for the accretion spots in polars (Woelk and Beuermann 1996). A map of the χ^2 distribution in the T_e–$\log \Lambda$ plane is presented in Fig. 6. The presented χ^2 values are the minimum ones for each pair (T_e, $\log \Lambda$) and were found by optimization for the magnetic field strength B, the angle θ, and the contribution of the Rayleigh–Jeans component to the total radiation from the system. Unfortunately, because of the roughness of the adopted model, it is difficult to limit the range of admissible values with reliable significance levels. Therefore, we restricted ourselves to specifying the region in the χ^2 distribution in which the amplitude of the cyclotron harmonics is described with an accuracy better than ≈50% (see Fig. 6). The angle θ was found to belong to the range from 50° to 70°. Figure 5 shows the description of the observed spectrum by the cyclotron spectrum at $T_e =$ 10 keV. The magnetic field strength $B = 34 \pm 2$ MG found from the cyclotron spectrum is higher than the estimate obtained from the analysis of the Zeeman splitting by ≈6 MG. Such discrepancies in the results of the two methods are typical for AM Her systems. The magnetic field averaged over the stellar disk is found when analyzing the photospheric lines of a white dwarf, whereas the magnetic strength near the magnetic pole is determined from the cyclotron harmonics. The latter estimate should definitely be greater than the former one, as observed in the case of J0854.

Doppler Tomography

The Doppler tomograms represent the distribution of emission line sources in two-dimensional velocity space. Each point of this space is specified by a pair of polar coordinates: the absolute velocity relative to the system's center of mass v in projection onto the orbital plane (to within the factor $\sin i$, where i is the orbital inclination) and the angle ϑ specifying the direction of the velocity vector in the orbital plane (this angle is usually measured from the line connecting the centers of mass of the stellar components). For details in the interpretation of Doppler tomograms, see Marsh and Schwope (2016) and Kotze et al. (2015, 2016). Since we do not have the orbital ephemeris of J0854, the tomograms were reconstructed to within the rotation angle, i.e., the angle ϑ of the tomogram points was determined to within a constant term. The tomography for J0854 was performed in the Hβ line, in which the maximum signal-to-noise ratio in the two series of observations is achieved. The Doppler tomograms were reconstructed using the code from Kotze et al. (2015), which implements the maximum entropy method.

The tomograms of J0854 are presented in Fig. 7 in two projections: standard and inside–out. In the first projection the velocity v increases from the center of the tomogram to its periphery. In the inside–out projection, on the contrary, the absolute velocity increases from the periphery to the center. The latter option is preferable for studying high-velocity structures that would be smeared over a large area in the standard projection (for details on this effect, see Kotze et al. 2015). For the convenience of comparing the tomograms obtained on different nights, we represented the intensity distribution from the April 24/25, 2022 data by a set of isolines. We superimposed these isolines on the map obtained from the March 7/8, 2022 spectra presented in color gradations.

The tomograms of J0854 are typical for AM Her systems. There is an intensity maximum in the fourth quadrant of the standard tomogram and a weaker bright region in the first quadrant elongated in the

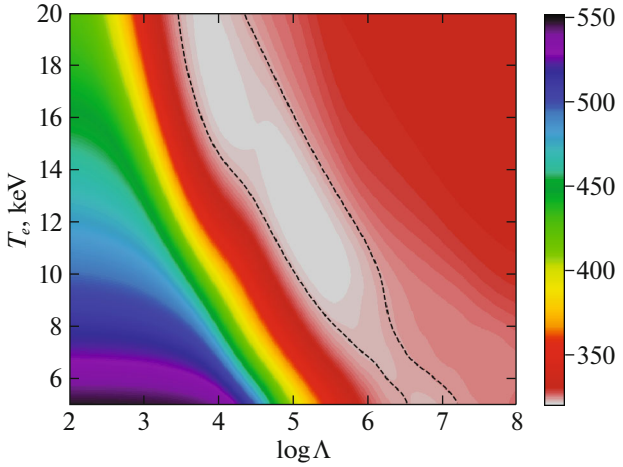

Fig. 6. A map of the χ^2 distribution in the T_e–log Λ plane. The black dashed isolines highlight the χ^2 value at which the amplitudes of the cyclotron harmonics are described with an accuracy ∼ 50%.

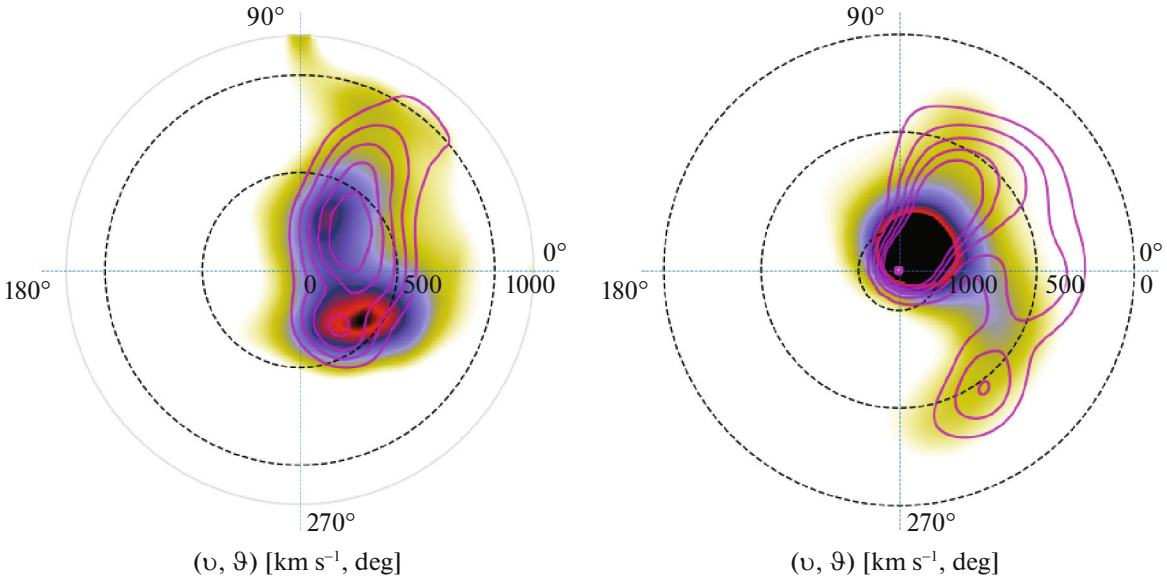

Fig. 7. Doppler tomograms of J0854 in the Hβ line. The left and right panels present the tomograms in the standard and inside–out projections, respectively. The tomograms reconstructed from the March 7/8, 2022 spectra are presented in color gradations, while the April 24/25, 2022 tomograms are represented by the isolines. The tomograms are given in polar coordinates: the dashed circumferences indicate the regions with a constant velocity magnitude (v = 0, 500, 1000 km s^{-1}); the polar angles (ϑ = 0, 90, 180, 270°) specifying the direction of motion of the emitting particles are marked near the periphery of the tomograms.

radial direction. The same picture is also observed on the map in the inside–out projection, but it differs by a more pronounced high-velocity component. Recalling that the Doppler maps were reconstructed to within the rotation angle, we could rotate them through ∼ 180° and see their correspondence to the maps of other polars, for example, HU Aqr (Schwope et al. 1997) and BS Tri (Kolbin et al. 2022). The maximum in the fourth quadrant of the tomogram in the standard projection occurring at a velocity magnitude $v = 200–450$ km s^{-1} is probably formed near the Lagrange point L_1. The ballistic segment of the accretion stream can be its source. Part of the radiation can be produced in the reradiation region on the donor surface, but it cannot be dominant due to the absence of characteristic narrow components in the spectral

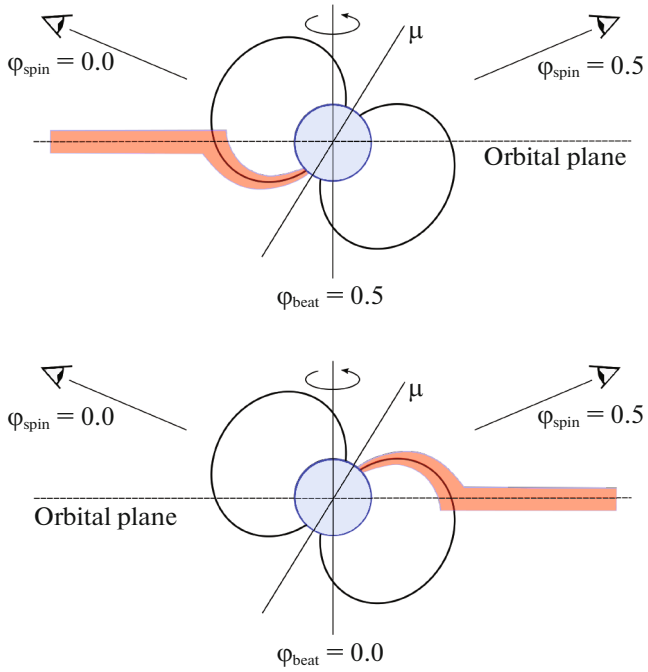

Fig. 8. Scheme for interpreting the photometric observations of J0854. Accretion onto the white dwarf in the low ($\varphi_{\rm beat} = 0.5$) and high ($\varphi_{\rm beat} = 0.0$) states is shown. In the low state accretion occurs near the rotation pole turned away from the observer. After half of the beat period, the magnetic dipole is oriented toward the inflowing gas by the opposite magnetic pole, which has better visibility conditions. In this case, the rotation phase of the white dwarf at which the accreting pole is visible changes from $\varphi_{\rm spin} = 0$ to $\varphi_{\rm spin} = 0.5$.

line profiles (Kolbin et al. 2022). The maximum in the first quadrant, which has an absolute velocity lower by $\Delta v \approx 50$ km s^{-1} and a polar angle larger by $\Delta\vartheta \approx 90°$, is probably formed in the segment of the accretion stream flowing along the magnetic field lines of the white dwarf. The decrease in the absolute velocity in this case is caused by the deceleration of the accretion stream near the stagnation region, where the ram pressure of the stream becomes equal to the magnetic pressure ($\rho v^2 = B^2/8\pi$, where ρ is the stream density). After this region, the gas moves along the magnetic field lines with the appearance of a velocity component that is perpendicular to the orbital plane (if the magnetic dipole axis lies in the orbital plane) and is not detected in Doppler tomography. The abrupt change in the angle ϑ can be interpreted as a rapid change in the direction of the stream during the transition from the ballistic trajectory to the magnetic one.

The phases of the beat period at the times of our spectroscopic observations are $\varphi_{\rm beat} = 0.91 \pm 0.09$ and $\varphi_{\rm beat} = 0.87 \pm 0.1$ for the March and April observations, respectively. The error in the beat period is responsible for the high uncertainty in the phase. The two series of spectroscopic observations differ by $\Delta\varphi_{\rm beat} = 0.04$. It seems that such a phase difference is not enough to distinguish the differences in the accretion flow. Although the Doppler tomograms also have different positions of the intensity maxima (this is especially clearly seen on the maps in the standard projection), these differences can be caused by incomplete coverage of the orbital period in the March observations ($0.6P_{\rm orb}$).

CONCLUSIONS

We discovered a new asynchronous polar, J0854. A beat period $P_{\rm beat} = 24.6 \pm 0.1$ days is distinguished in its long-term ZTF light curves. During this period the polar changes its mean brightness from $\langle g \rangle \approx 19.5^m$ (low state) to $\langle g \rangle \approx 16.5^m$ (high state). An analysis of the light curves in the low and high states revealed the rotational variability of the white dwarf with a period $P_{\rm spin} = 113.197 \pm 0.001$ min. The orbital period $P_{\rm orb} = 113.55984 \pm 0.001$ min and the sidebands arising from the modulation of the rotational variability by the orbital motion also manifest themselves in the periodograms for the low and high states. The asynchrony of J0854 is $(\Omega - \omega)/\Omega \approx 0.3\%$ and is consistent with the values of this parameter for asynchronous polars, where it is $<2\%$. The light curve of J0854 in the low state folded with

the rotation period has a double-peaked bright phase that is interpreted as the passage of the cyclotron radiation source (i.e., the accretion spot) across the white-dwarf disk. A similar shape of the light curve is also observed in the high state, but it is shifted by about half the rotation period. This effect can be interpreted as a change of the main accreting pole as the state changes from low to high. Since the mean brightness of the polar in the high state is higher by $\approx 3^m$, it can be assumed that the accreting pole in it has better visibility conditions, i.e., it is located near the rotation pole facing the observer. In addition, the differences in the brightnesses of the two states can be associated with the possible difference in the magnetic field strengths at the magnetic poles. In this case, since in the high state the brightness does not drop to the level of the low state, the accretion spot probably does not go behind the white-dwarf disk. The latter implies that the inclination of the dipole to the rotation axis is $\beta < 90^\circ - i$, where i is the inclination of the rotation axis to the line of sight. The described scheme of accretion in J0854 is shown in Fig. 8.

There are Zeeman splitting components of the Hβ line in the spectra of J0854. Based on them, we estimated the magnetic field of the white dwarf to be $B = 28.5 \pm 1.5$ MG. Cyclotron harmonics whose positions correspond to a magnetic field $B = 34 \pm 2$ MG were detected in one of the spectra. The higher estimate of the magnetic field strength stems from the fact that it was obtained for a region close to the magnetic pole, whereas the magnetic field strength averaged over the stellar surface is found from the Zeeman splitting. Our Doppler tomograms show a distribution of emission line sources typical for polars, on which low-velocity structures probably forming near the ballistic trajectory and high-velocity features probably originating in the white-dwarf magnetosphere manifest themselves. No significant differences in the tomograms obtained in different periods were found. This is apparently due to the small difference in beat phase between the spectral series.

The polar J0854 is an interesting object for further optical observations. For example, to test the hypothesis of switching between the main accreting poles, polarization observations at different phases of the beat period are desirable. When accretion changes from one pole to another, a reversal of the sign of circular polarization is to be expected. It would be interesting to carry out additional phase-resolved spectroscopic observations. The Doppler maps obtained on their basis would allow the changes in the geometry of the accretion flows during the rotation of the magnetic dipole relative to the donor to be investigated.

FUNDING

This study was supported by the Russian Science Foundation grant no. 22-72-10064, https://rscf.ru/project/22-72-10064/. The observations with the telescopes at the Special Astrophysical Observatory of the Russian Academy of Sciences are supported by the Ministry of Science and Higher Education of the Russian Federation. The instrumentation is updated within the "Science and universities" National Project.

CONFLICT OF INTEREST

The authors of this work declare that they have no conflicts of interest.

REFERENCES

1. V. L. Afanasiev and A. V. Moiseev, Baltic Astron. **20**, 363 (2011).
2. K. Beuermann, V. Burwitz, K. Reinsch, A. Schwope, and H.-C. Thomas, Astron. Astrophys. **634**, 91 (2020).
3. R. K. Campbell, T. E. Harrison, A. D. Schwope, and St. B. Howell, Astrophys. J. **672**, 531 (2008).
4. G. Chanmugam and G. A. Dulk, Astrophys. J. **244**, 569 (1981).
5. D. J. Christian, N. Craig, J. Dupuis, and B. Roberts, Inform. Bull. Var. Stars **5032**, 1 (2001).
6. M. Cropper, Space Sci. Rev. **54**, 195 (1990).
7. M. Dillon, B. T. Gänsicke, A. Aungwerojwit, P. Rodríguez-Gil, T. R. Marsh, S. C. C. Barros, P. Szkody, S. Brady, T. Krajci, and A. Oksanen, Mon. Not. R. Astron. Soc. **386**, 1568 (2008).
8. P. G. van Dokkum, Publ. Astron. Soc. Pacif. **113**, 1420 (2001).
9. J. P. Halpern, S. Bogdanov, and J. R. Thorstensen, Astrophys. J. **838**, 124 (2017).
10. S. Hellier, *Cataclysmic Variable Stars* (Springer, London, 2001).
11. K. Horne, Publ. Astron. Soc. Pacif. **98**, 609 (1986).
12. A. R. King and J. P. Lasota, Astrophys. J. **378**, 674 (1991).
13. A. I. Kolbin, N. A. Serebryakova, M. M. Gabdeev, and N. V. Borisov, Astrophys. Bull. **74**, 80 (2019).
14. A. I. Kolbin and N. V. Borisov, Astron. Lett. **46**, 812 (2020).
15. A. I. Kolbin, N. V. Borisov, N. A. Serebriakova, V. V. Shimansky, N. A. Katysheva, M. M. Gabdeev, and S. Yu. Shugarov, Mon. Not. R. Astron. Soc. **511**, 20 (2022).
16. E. J. Kotze, S. B. Potter, and V. A. McBride, Astron. Astrophys. **579**, 77 (2015).
17. E. J. Kotze, S. B. Potter, and V. A. McBride, Astron. Astrophys. **595**, 47 (2016).
18. C. Littlefield, P. Garnavich, K. Mukai, P. A. Mason, P. Szkody, M. Kennedy, G. Myers, and R. Schwarz, Astrophys. J. **881**, 141 (2019).
19. C. Littlefield, K. Mukai, R. Mumme, R. Cain, K. C. Magno, T. Corpuz, D. Sandefur, D. Boyd, M. Cook, J. Ulowetz, and L. Martinez, Mon. Not. R. Astron. Soc. **449**, 3107 (2015).

20. C. Littlefield, P. Garnavich, K. Mukai, P. A. Mason, P. Szkody, M. Kennedy, G. Myers, and R. Schwarz, Astrophys. J. **881**, 141 (2019).
21. C. Littlefield, D. W. Hoard, P. Garnavich, P. Szkody, P. A. Mason, S. Scaringi, K. Ilkiewicz, M. R. Kennedy, S. A. Rappaport, and R. Jayaraman, Astron. J. **165**, 43 (2023).
22. C. Littlefield, P. A. Mason, P. Garnavich, P. Szkody, J. Thorstensen, S. Scaringi, K. Ilkiewicz, M. R. Kennedy, and N. Wells, Astrophys. J. Lett. **943**, L24 (2023).
23. T. R. Marsh and A. D. Schwope, Astrophys. Space Sci. Libr. **439**, 195 (2016).
24. F. Masci, R. Laher, B. Rusholme, et al., Publ. Astron. Soc. Pacif. **131**, 995 (2018).
25. J. Patterson, Publ. Astron. Soc. Pacif. **106**, 209 (1994).
26. E. P. Pavlenko, P. A. Mason, A. A. Sosnovskij, S. Yu. Shugarov, J. V. Babina, K. A. Antonyuk, M. V. Andreev, N. V. Pit, O. I. Antonyuk, and A. V. Baklanov, Mon. Not. R. Astron. Soc. **479**, 341 (2018).
27. C. Schimeczek and G. Wunner, Astrophys. J. Suppl. Ser. **212**, 26 (2014).
28. A. D. Schwope, K. H. Mantel, and K. Horne, Astron. Astrophys. **319**, 894 (1997).
29. A. Silber, H. V. Bradt, M. Ishida, T. Ohashi, and R. A. Remillard, Astrophys. J. **389**, 704 (1992).
30. A. V. Sobolev, A. G. Zhilkin, D. V. Bisikalo, and D. A. H. Buckley, Astron. Rep. **65**, 392 (2021).
31. H. S. Stockman, G. D. Schmidt, and D. Q. Lamb, Astrophys. J. **332**, 282 (1988).
32. P. Szkody, A. Henden, O. J. Fraser, N. M. Silvestri, G. D. Schmidt, J. J. Bochanski, M. A. Wolfe, M. Agueros, et al., Astron. J. **129**, 2386 (2005).
33. G. Tovmassian, D. González-Buitrago, J. Thorstensen, E. Kotze, H. Breytenbach, A. Schwope, F. Bernardini, S. V. Zharikov, et al., Astron. Astrophys. **608**, A36 (2017).
34. J. T. VanderPlas, Astrophys. J. Suppl. Ser. **236**, 16 (2018).
35. B. Warner, *Cataclysmic Variable Stars* (Cambridge Univ. Press, Cambridge, 1995).
36. U. Woelk and K. Beuermann, Astron. Astrophys. **306**, 232 (1996).

Translated by V. Astakhov